Quantum metrology algorithms for dark matter searches with clocks

M. H. Zaheer,[1,*] N. J. Matjelo,[2] D. B. Hume,[3] M. S. Safronova,[1,4] and D. R. Leibrandt[3,5,6,†]

[1]*Department of Physics and Astronomy, University of Delaware, Delaware 19716, USA*
[2]*Department of Physics and Electronics, National University of Lesotho, Roma 180, Lesotho*
[3]*Time and Frequency Division, National Institute of Standards and Technology, Boulder, Colorado 80302, USA*
[4]*Joint Quantum Institute, NIST and the University of Maryland, College Park, Maryland 20742, USA*
[5]*Department of Physics and Astronomy, University of California, Los Angeles, California 90095, USA*
[6]*Department of Physics, University of Colorado, Boulder, Colorado 80309, USA*

(Received 2 December 2023; accepted 23 October 2024; published 2 January 2025)

Quantum algorithms such as dynamical decoupling can be used to improve the sensitivity of a quantum sensor to a signal while suppressing sensitivity to noise. Atomic clocks are among the most sensitive quantum sensors, with recent improvements in clock technology allowing for unprecedented precision and accuracy. These clocks are highly sensitive to variations in fundamental constants, making them ideal probes for local ultralight scalar dark matter. Further improvements to the sensitivity are expected in proposed nuclear clocks based on a nuclear transition in the thorium-229 isotope. We investigate the use of various quantum metrology algorithms in the search for dark matter using quantum clocks. We propose a broadband dynamical decoupling algorithm and compare it with quantum metrology protocols that have been previously proposed and demonstrated, namely, differential spectroscopy and narrowband dynamical decoupling. We conduct numerical simulations of scalar dark matter searches with realistic noise sources and accounting for dark matter decoherence. Finally, we propose an alternative thorium nuclear transition excitation method that bypasses the technical challenges associated with vacuum ultraviolet lasers.

DOI: 10.1103/PhysRevA.111.012601

I. INTRODUCTION

The extraordinary improvement in the precision of atomic clocks over the last 15 years [1,2] has put clocks in an uncharted territory in which the fundamental postulates of modern physics are untested. For example, if fundamental constants, such as the fine-structure constant α, are space-time dependent, then so are the atomic, molecular, and nuclear transition frequencies. Variations of fundamental constants would change the ticking rate of clocks and make them depend on the location, time, or type of clock since the frequencies of different clocks depend differently on the fundamental constants.

Ultralight scalar fields arise in many theories beyond the Standard Model [3,4] and may source variations of fundamental constants that affect atomic clock frequencies [5,6]. Such particles can also be dark matter (DM), which makes 85% of all matter in the Universe, but it is of yet unknown origin. In our galaxy, such dark matter exhibits coherence and behaves like a wave with an amplitude $\sim\sqrt{\rho_{\rm DM}}/m_\phi$, where $\rho_{\rm DM} = 0.4\,{\rm GeV/cm^3}$ is the local DM density and m_ϕ is the DM particle mass [6]. The coupling of such DM to the Standard Model leads to oscillations of fundamental constants, and therefore, clock transition frequencies. Since different clocks have different sensitivities to such effects, measurements of the ratio of two clock frequencies over time can be used to extract an oscillation signal at the DM Compton frequency for a wide range of DM masses and interaction strengths [6–8]. These advances started a new era of clock experiments aimed at detecting dark matter, with several ongoing searches [4].

It was recently suggested that ultralight DM can form gravitationally bound objects that may be trapped by an external gravitational potential, such as that of the Earth or the Sun [9]. It was shown in Ref. [10] that such a halo can have extremely large DM overdensities, up to 17 orders of magnitude at 0.1 AU from the Sun, drastically increasing the discovery potential. Tsai *et al.* [10] proposed a clock-comparison satellite mission with two clocks onboard, to the inner reaches of the solar system to search for a dark matter halo bound to the Sun and look for the spatial variation of the fundamental constants associated with a change in the gravitational potential. However, in this scenerio, the DM distribution peaks for about 10^{-13} eV DM masses ($\sim$24 Hz), at which clocks lose sensitivity due to the probe duration of the clocks. In this work, we explore different quantum algorithms for clock operation and propose a broadband dynamic decoupling scheme that allows one to reach such masses without significant losses of sensitivity.

Here, we consider the linear coupling of ultralight scalar dark matter ϕ with the photon field, which, by using the convention of Ref. [11], is given by the interaction Lagrangian [6,11]

$$\mathcal{L}_{\phi\gamma} = \kappa\phi\frac{d_e}{4e^2}F^{\mu\nu}F_{\mu\nu}, \tag{1}$$

where $\kappa = \sqrt{4\pi}/M_{Pl}$ with $M_{\rm Pl}$ being the Planck mass, e is the electron charge, and d_e is the (dimensionless) dark

*Contact author: hani@udel.edu
†Contact author: leibrandt@ucla.edu

matter-QED coupling constant. We use natural units in the introduction unless otherwise specified. The present day solution for ϕ, assuming negligible self-interactions, is given by [6]

$$\phi = \phi_0 \cos\left(m_\phi t - \vec{k}_\phi \cdot \vec{x} + \cdots\right). \tag{2}$$

Here, the amplitude $\phi_0 = \sqrt{2\rho_{\rm DM}}/m_\phi$, the wave vector magnitude is determined by the virial velocity $|\vec{k}_\phi| = v_{\rm vir} m_\phi \approx 10^{-3} m_\phi$, and $\cdots$ represents higher-order terms in the relativistic expansion. The dark matter-QED coupling is determined by

$$d_e = \frac{\partial \ln \alpha}{\partial(\kappa\phi)}. \tag{3}$$

Integrating this, we obtain

$$\alpha = \alpha_0(1 + d_e \kappa \phi), \tag{4}$$

where α_0 is the bare (unperturbed) fine-structure constant.

The sensitivity of an optical clock to any variation of α is quantified by the dimensionless enhancement factor K. Clocks with the best stability, total systematic uncertainty, and the highest possible values of $\Delta K = K_1 - K_2$ for clocks 1 and 2 have the highest discovery potential. The K factors are small, 0.008–1.0, for all current clocks based on optical lattices and most trapped ion clocks, with the exception of the Hg^+ quadrupole ($K = -3$) and Yb^+ octupole clock ($K = -6$) transitions [12]. Clocks based on nuclear transitions can have much higher sensitivities to variations in the fundamental constants [13]. For a thorium isomer nuclear clock, the clock transition frequency depends on the fine-structure constant $\nu \propto \alpha^K$, with $K = 5900(2300)$ [14]. The fractional amplitude of oscillations of the clock transition frequency can be given as a function of the QED-dark matter coupling constant

$$K d_e \kappa \phi_0 = K d_e \frac{6.4 \times 10^{-31}\,\text{eV}}{m_\phi}. \tag{5}$$

From here onwards m_ϕ is understood to be in units of eV. The smaller the minimum detectable oscillation amplitude, the lower the value of d_e can be probed from the experiment.

The transition frequencies of nuclear energy levels are well outside the laser-accessible range, by four to six orders of magnitude, with a single exception of the ^{229}Th nuclear isomer transition. Designing a clock based on this ultranarrow nuclear transition [15,16] is particularly attractive due to its insensitivity to many systematic effects. In addition to α, this transition is predicted to have a very large sensitivity to variations in $m_q/\Lambda_{\rm QCD}$ [13,17], where m_q are the quark masses and $\Lambda_{\rm QCD}$ parameterizes the strength of the strong force, larger than all present atomic clocks.

Recently, significant experimental progress has been made in the development of a thorium nuclear clock [18–21]. In 2024, laser excitation of the ^{229}Th nuclear transition was demonstrated for the first time in Th-doped CaF_2 crystals using a table-top tunable laser system [19]. The nuclear resonance for Th^{4+} ions in Th:CaF_2 is measured at the wavelength 148.3821(5) nm, with the fluorescence lifetime in the crystal is 630(15) s, corresponding to a lifetime of 2510(60) s for a nucleus isolated in a vacuum. Shortly after, a frequency-stabilized VUV frequency comb was used to improve frequency resolution by $\sim 10^6$ and directly resolve nuclear quadrupole splitting in Th-doped CaF_2 [21]. The nuclear transition frequency was determined to be 2 020 407 384 335(2) kHz. The ratio of the isomer and ground-state quadrupole moments was also determined in Ref. [21] from the precise measurement of the nuclear quadrupole splittings. This enabled an estimate of the sensitivity K using a geometric model [14].

The mass of ultralight scalar dark matter particles is unknown over a very large range corresponding to a Compton frequency anywhere from μHz to THz. Typically, optical clocks are operated in a manner that is optimized to reach the highest possible precision for measuring static frequency differences or ratios at asymptotically long averaging times. This is achieved by probing the clock transition using Rabi or Ramsey spectroscopy with as long of a probe duration as possible while maintaining coherence between the clock laser and the atoms. These measurements are sensitive to oscillations at frequencies below the recriprocal of the probe duration of order 1 Hz.

The fundamental limit to the measurement precision is set by quantum projection noise, and, for clocks based on unentangled atoms, this limit is referred to as the standard quantum limit (SQL), with uncertainty $\sigma_{\rm SQL} \propto 1/\sqrt{T_p}$, where T_p is the probe duration. Thus, extending T_p improves the sensitivity of dark matter searches for light particle masses. For several highly forbidden clock transitions, the atomic coherence time can be orders of magnitude longer than that of the best present-day clock lasers, so laser noise sets the experimental limit to measurement precision.

For frequency ratio measurements between two optical clocks, a new technique called differential spectroscopy (DS) has recently been proposed [22] and demonstrated [23] which circumvents the laser coherence time limit to the probe duration. In differential spectroscopy, the two clocks are probed synchronously using lasers that are phase locked to a common frequency comb, such that the correlated laser noise can be circumvented. We focus on the case of frequency ratio measurements between an optical lattice clock and a trapped ion clock. The probe duration of the ion clock can be extended all the way to its atomic coherence time if the lattice clock is operated with two atomic ensembles probed alternately to achieve a zero-dead-time measurement of the laser phase [see Fig. 1(a)]. Zero-dead-time differential spectroscopy is a promising technique for ultralight scalar dark matter searches at the low particle mass limit, which would manifest as slow oscillations in the frequency ratio between thorium nuclear transition or ytterbium octupole transition trapped-ion clocks with a large sensitivity to the DM field, and strontium or ytterbium optical lattice clocks with a small sensitivity that would serve as the stable reference. As shown in the right panel of Fig. 1(a), clocks operated using differential spectroscopy (and also standard Rabi or Ramsey spectroscopy) are primarily sensitive to oscillations at frequencies lower than the reciprocal of the clock probe duration, with the sensitivity decreasing rapidly with increasing frequency above this cutoff. While the sensitivity at frequencies higher than the inverse probe duration can be improved by reducing the probe duration, this comes at the cost of lower sensitivity at low frequencies.

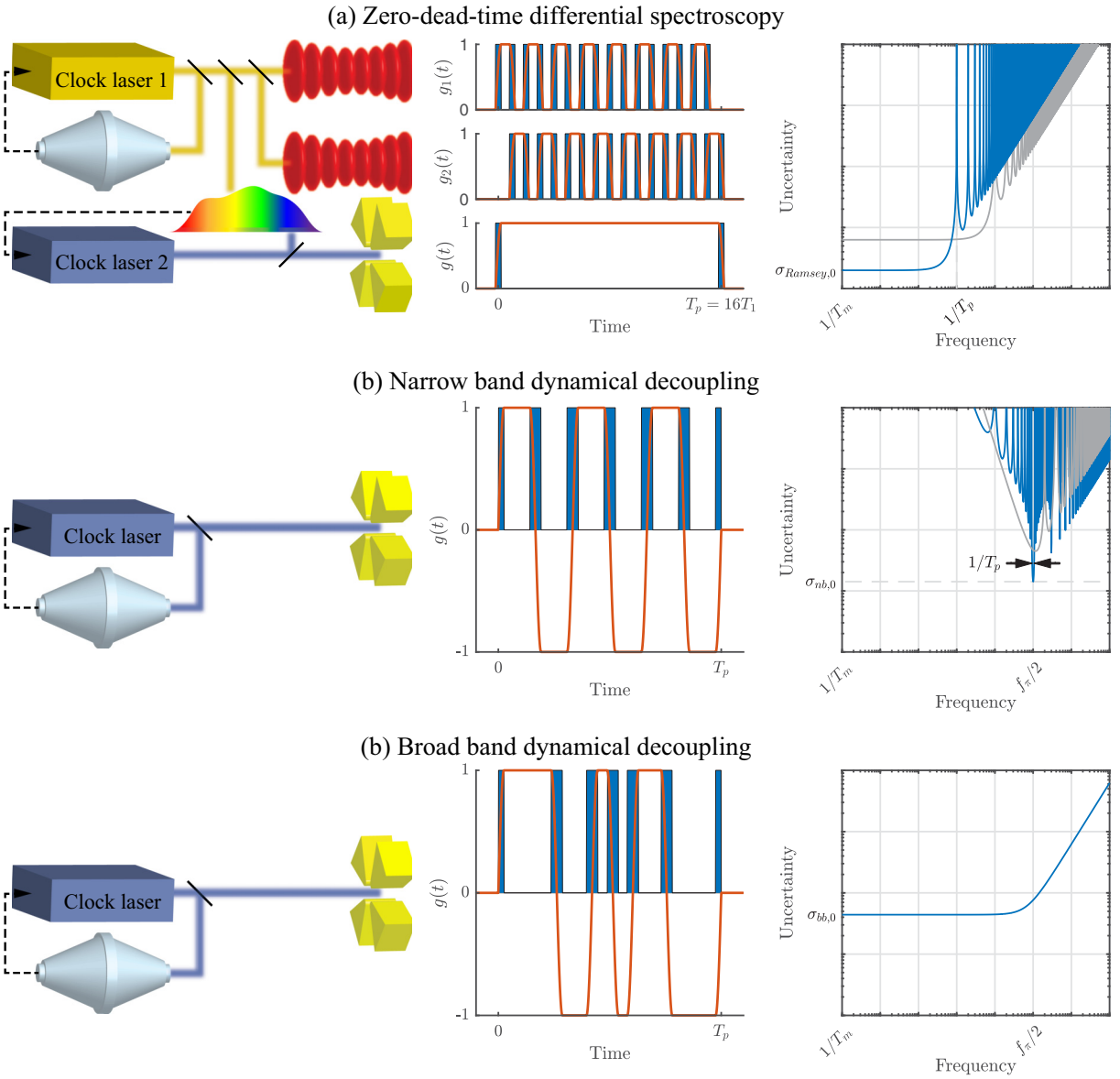

FIG. 1. Diagrams of experimental setups (left), pulse sequences (middle), and examples of theoretical sensitivity plots (right) for different quantum metrology algorithms: (a) zero-dead-time differential spectroscopy, (b) narrowband dynamical decoupling, and (c) broadband dynamical decoupling. Clock lasers are depicted as blue and yellow boxes; optical cavities used to stabilize the clock lasers are depicted as light gray cylinders with conical ends; feedback paths are indicated by black dashed lines; ensembles of atoms confined in optical lattices are depicted as stacks of red disks; and ions confined in ion traps are depicted as four yellow trap electrodes. The pulse sequences depict $\pi/2$ and π pulses as blue rectangles with increasing time from left to right. The sensitivity $g(t)$ of the pulse sequence to clock transition or laser frequency fluctuations as a function of the time of the frequency fluctuations during the pulse sequence is shown as a red line. The sensitivity plots show the theoretical minimum detectable fractional amplitude of an oscillating signal as a function of the oscillation frequency, such that higher sensitivity is indicated by the curve being lower on the plot. f_π is the frequency of π pulses, T_m is the total duration of the measurement campaign, and T_p is the probe duration, i.e., the time between the two Ramsey $\pi/2$ pulses before the state of the atoms is measured. The gray curves show how the sensitivity changes when T_p is decreased by a factor of 10. The sensitivity for BBDD does not depend on T_p. All sensitivity plots depict the same range of frequencies and sensitivities, with both axes being logarithmic.

Dynamical decoupling can be used to shift the sensitivity of clock-based dark matter searches to higher oscillation frequencies. Ramsey pulse sequences with π pulses inserted into the free evolution time [see Fig. 1(b)] are used to dynamically decouple noise from the signal in a quantum system. The first use of dynamical decoupling was in nuclear magnetic resonance, with the spin echo effect [24]. It was introduced in quantum information research as a means of dealing with decoherence and dissipation [25].

A well-established dynamical decoupling pulse sequence known as Car-Purcell-Meiboom-Gill (CPMG) is a technique that is a quantum analog of the classical lock-in amplifier [26,27]. An ion in $|\uparrow\rangle$ is prepared in a superposition state $(|\uparrow\rangle + |\downarrow\rangle)/2$ by using a $\pi/2$ pulse. During the probe, a series

of regularly spaced π pulses are used to modulate the sign of sensitivity to atomic or laser frequency fluctuations. A final $\pi/2$ pulse completes the pulse sequence. This sequence is sensitive to oscillations over a narrow range of frequencies near one half of the frequency of the π pulses [Fig. 1(b)]. This method was demonstrated on a $^{88}Sr^{+}$ ion by Kotler *et al.* [28] and analyzed in the context of dark matter searches by Aharony *et al.* [29]. To distinguish this method from the new dynamical decoupling algorithm introduced below, we henceforth refer to CPMG as narrowband dynamical decoupling (NBDD).

In the present work, we propose and evaluate a broadband dynamical decoupling (BBDD) scheme that allows us to probe higher dark matter masses and resolves the disadvantages of DS and NBDD schemes. We review each scheme. Then, we evaluate the performance of all three schemes in realistic numerical simulations based on the thorium nuclear isomer transition. We highlight the sensitivity of thorium nuclear clocks for dark matter searches in our simulations due to large sensitivity factor to variations in the fine-structure constant, $K = 5900(2300)$ [14], to demonstrate the potential reach of the quantum clock technologies for dark matter searches, but these algorithms are equally applicable for existing and future atomic clocks. The simulation results are compared to contemporary dark matter search experimental results and other proposals. Finally, an alternative nuclear excitation scheme in thorium is presented.

II. DARK MATTER SEARCH ALGORITHMS

A. Dark matter search coherent signal analysis

For a given clock transition frequency ν_0 and neglecting decoherence, dark matter induces a sinusoidal change in frequency of amplitude ν_S, oscillation frequency f, and random phase θ given by

$$\nu(t) = \nu_0 + \nu_S \cos(2\pi f t + \theta). \tag{6}$$

Here onward, SI units are used unless otherwise stated.

The phase of the atomic superposition state in the rotating frame accumulated during the jth probe is

$$\phi_j = \int_{t_j - T_p/2}^{t_j + T_p/2} 2\pi g(t)\nu(t)dt, \tag{7}$$

where $t_j = jT_p$ is the time at the middle of the probe and T_p is the probe duration, i.e., the time between the two Ramsey $\pi/2$ pulses before the state of the atoms is measured. The sensitivity function [30] is defined as the relative variation in transition probability p due to the infinitesimal phase step $\delta\phi$: $g(t) = 2\lim_{\delta\phi\to 0}\frac{\delta p}{\delta\phi}$. It determines the change in the atomic transition probability p caused by a detuning $\nu(t) = \nu_S\cos(2\pi f t + \theta) + \nu_{LN}(t)$ between the ion transition frequency and the laser frequency, where $\nu_{LN}(t)$ is the laser frequency noise.

The sensitivity function is time dependent and can be set to any value between -1 and 1 by applying laser pulses that change the orientation of the Bloch vector. A standard Ramsey sequence, for example, consists of two $\pi/2$ pulses separated by the total sequence duration T. We use the convention that the first $\pi/2$ pulse rotates the Bloch vector by $\pi/2$ radians about the x axis, and the second $\pi/2$ pulse rotates the Bloch vector by $\pi/2$ radians about the y axis. (Here, we assume that the durations of the laser pulses are much shorter than the total sequence duration and can be neglected.) The Ramsey algorithm has a sensitivity function $g(t) = +1$ for the duration of the sequence and is therefore optimal for the detection of a time-independent detuning. The sign of the sensitivity function can be flipped by applying π pulses about the x axis during a Ramsey sequence.

For a deterministic frequency oscillation with amplitude ν_S at frequency f [Eq. (6)], the phase accumulated during the jth probe

$$\begin{aligned}\phi_{S,j}^{\mathrm{det}}(f) &= 2\pi\nu_S\int_{t_j - T_p/2}^{t_j + T_p/2} g(t)\cos(2\pi f t + \theta)dt \\ &= 2\pi\nu_S[g_{I,j}\cos\theta - g_{Q,j}\sin\theta],\end{aligned} \tag{8}$$

where

$$\begin{aligned}g_{I,j}(f) &= \int_{t_j - T_p/2}^{t_j + T_p/2} g(t)\cos(2\pi f t)dt \quad \text{and} \\ g_{Q,j}(f) &= \int_{t_j - T_p/2}^{t_j + T_p/2} g(t)\sin(2\pi f t)dt\end{aligned} \tag{9}$$

are the in-phase and quadrature components of the sensitivity function of the jth probe. Here, integration is performed over the duration of the jth probe. Ultralight DM induces oscillations of the transition frequency that are stochastic in nature with a nonzero linewidth [31]. In this case, the phase accumulated due to the dark matter signal is given by

$$\phi_{S,j} = \int_{t_j - T_p/2}^{t_j + T_p/2} 2\pi g(t)\nu_S(t)dt, \tag{10}$$

where $\nu_S(t)$ is the detuning caused by the dark matter field.

The measured phase for the jth probe $\phi_{M,j} = \phi_{\mathrm{QPN},j} + \phi_{LN,j} + \phi_{S,j}$ where $\phi_{\mathrm{QPN},j}$ and $\phi_{LN,j}$ are the contributions due to quantum projection noise and laser noise, respectively. All these contributions are random variables centered on zero. Motivated by Eqs. (8) and (9), at the end of a measurement campaign consisting of $N_p = T_m/T_p$ probes, we compute the measured signal ϕ_M as a function of the analysis frequency f by adding the phases of each probe with modulation-frequency-dependent signs, so that the signal contribution adds coherently

$$\begin{aligned}(\phi_M)^2 = &\frac{1}{2}\left(\sum_{j=0}^{N_p-1}\mathrm{sgn}[g_{I,j}(f)]\phi_{M,j}(f_{\mathrm{DM}})\right)^2 \\ &+ \frac{1}{2}\left(\sum_{j=0}^{N_p-1}\mathrm{sgn}[g_{Q,j}(f)]\phi_{M,j}(f_{\mathrm{DM}})\right)^2.\end{aligned} \tag{11}$$

This equation defines a coherent analysis of all probes together and is new in this work. The contributions from noise sources are independent of the dark matter signal contribution and thus add incoherently.

The expectation value of the minimum detectable fractional signal amplitude ν_S/ν_0 for coherent oscillations of the

transition frequency at f can be written as

$$\sigma(f) = \frac{1}{\nu_0}\sqrt{\frac{\langle(\phi_N)^2\rangle}{\langle(\phi_S/\nu_S)^2\rangle}}. \tag{12}$$

Here ϕ_S (ϕ_N) is the total accumulated phase due to signal (noise). In the following, we refer to this quantity as the sensitivity.

B. Ramsey or differential spectroscopy

In differential spectroscopy [Fig. 1(a)], the sensitivity to deterministic oscillations of the ion clock transition frequency is equivalent to that of the standard Ramsey spectroscopy, with the key distinction that in differential spectroscopy (DS), the ion clock probe duration T_p is not limited by the laser coherence time, which limits the probe time in standard Ramsey spectroscopy. Extending the probe duration results in improved sensitivity to low-frequency oscillations and reduced sensitivity to oscillations at frequencies larger than $1/T_p$. In the oscillation frequency range $1/T_m \ll f \ll 1/T_p$ where T_m is the total duration of the measurement campaign, the sensitivity to deterministic oscillations of unknown phase θ is given by [31]

$$\sigma_{\text{Ramsey}}(f) = \sigma_{\text{Ramsey},0}\frac{\pi f T_p}{|\sin(\pi f T_p)|}, \tag{13}$$

where

$$\sigma_{\text{Ramsey},0} = \frac{X_{\text{Ramsey}}}{2\pi\nu_0\sqrt{T_p T_m}}. \tag{14}$$

In the following, we refer to this quantity as the uncertainty. This defines the bounds that can be placed on the size of ν_S. X_{Ramsey} is an order unity constant that depends on the confidence interval and whether the search is for deterministic or stochastic signals. For deterministic signals and $X_{\text{Ramsey}} \approx 5.3$, the oscillation amplitude $|\nu_S| < \sigma_{\text{Ramsey}}(f)\nu_0$ with 95% confidence [31]. This is a measurement of the ion clock transition frequency with respect to the lattice clock transition frequency. In contrast, the dynamical decoupling sequences described below are measurements of the ion clock transition frequency with respect to the cavity resonance frequency.

C. Narrowband dynamical decoupling

Differential spectroscopy experiences a reduction in sensitivity at higher frequencies, especially at peaks of insensitivity that occur at integer multiples of $1/T_p$, which is a result of an integer number of dark matter oscillations fitting into the probe time. Narrowband dynamical decoupling in the style of Ref. [28] introduces π pulses during the probe to shift the sensitivity to higher oscillation frequencies, and a DM search based on this method was performed by Aharony *et al.* [29]. In Ref. [29], the rate of π pulses f_π was constant and the same for every probe, leading to a sensitivity plot with the shape shown in Fig. 1(b) given by [29,32]

$$\sigma_{nb}(f) = \sigma_{nb,0}\left|\frac{f T_p\cos(\pi f/f_\pi)}{\sin(\pi f T_p - \pi f_\pi T_p/2)\sin^2[\pi f/(2f_\pi)]}\right|, \tag{15}$$

where

$$\sigma_{nb,0} = \frac{X_{nb}}{2\pi\nu_0\sqrt{T_p T_m}}. \tag{16}$$

Furthermore, the data were analyzed under the assumption that the phase of the signal for each probe is uniformly distributed over 2π and there is no correlation of the phase between different probes. In this case $X_{nb} \approx 8.9$ corresponds to the 95% confidence interval. (Here, we use the Wilson confidence interval method [33], but other methods give similar results [34].) A downside of this protocol is that it offers improved sensitivity for signals with a only narrow frequency range $1/T_p$ centered at $f_\pi/2$. The latter problem can be overcome by randomly choosing a different value of f_π for each probe. Furthermore, the sensitivity can be further improved by analyzing all of the probes coherently by using knowledge of the correlation between the signal phase between probes using the method proposed above. This is the approach we adopt here, and we refer to this as narrowband dynamical decoupling (NBDD).

D. Broadband dynamical decoupling

For dark matter searches over a broad range of particle masses, corresponding to a wide range of detuning oscillation frequencies f_{DM}, we propose and analyze a broadband dynamical decoupling algorithm [Fig. 1(c)]. In this algorithm, π pulses about the x axis are inserted into a Ramsey sequence at random times with a distribution designed to maximize sensitivity to the oscillation frequency range of interest. Our numerical simulations are consistent with the emperical equation

$$\sigma_{bb}(f) = \sigma_{bb,0}\sqrt{1+\left(\frac{f}{f_\pi/2^{3/2}}\right)^2}, \tag{17}$$

where

$$\sigma_{bb,0} = \frac{X_{bb}}{2\pi\nu_0\sqrt{T_m/f_\pi}}. \tag{18}$$

In this case, f_π is the average frequency of π pulses. For deterministic signals and the 95% confidence interval, $X_{bb} \approx 4.8$. Notably, this limit does not depend on the probe duration T_p. Broadband dynamical decoupling (BBDD) offers similar advantages as NBDD with different random π pulse frequencies in each probe when searching for a signal with unknown frequency, but relaxes the requirements on laser coherence.

III. DARK MATTER SEARCH SENSITIVITY WITH THORIUM

We perform numerical simulations to determine the sensitivity of various quantum metrology algorithms to clock transition frequency oscillations induced by dark matter. In these simulations, we include realistic noise sources and the stochastic nature of scalar field dark matter.

The phase-accumulated during each probe due to laser frequency noise follows Eq. (7). For differential spectroscopy, because of the feedforward phase correction from the lattice clock, the effective laser phase noise is actually the quantum projection noise of the lattice clock. It is taken to be Gaussian

white noise with an Allan deviation set by the standard quantum limit for the lattice clock, which is taken to be a strontium lattice clock composed of 1000 atoms with a probe time of 1 s. For the dynamical decoupling algorithms, the laser frequency noise is taken to follow a $1/f$ power spectral density as is typical for cavity-stabilized lasers. The quantum projection noise in the clock contributes $\phi_{\mathrm{QPN},j} = \pm 1$, which is added to the laser frequency noise contribution to give the total phase accumulated due to noise in the jth probe $\phi_{N,j}$. The phase accumulated in each probe due to the dark matter signal $\phi_{S,j}$ is calculated accounting for the nonzero dark matter line width and decoherence, which are due to the dark matter velocity distribution. Further details pertaining to obtaining $\phi_{S,j}$ and $\phi_{N,j}$ are given in the Appendixes. We account for nonzero dark matter line width by analyzing over a range of analysis frequencies f around the dark matter Compton frequency f_{DM}. Then, the computed measurement result is fitted to the expected lineshape.

We run a detailed simulation for DS, NBDD, and BBDD. For each dark matter Compton frequency f_{DM}, we analyze 1000 frequency points f in the vicinity. The measurement time used is $T_m = 10^6$ s, and with a spectroscopy pulse sequence duration of $T_p = 1$ s, this translates into 10^6 simulated probes per analysis frequency. We use time steps of $0.1/f_{\mathrm{DM}}$ and $0.01/f_{\mathrm{DM}}$ for the dark matter line shape and laser frequency noise computations, respectively. The probe time used for differential spectroscopy, narrowband dynamical decoupling, and broadband dynamical decoupling searches are $T_p = 100$ s, $T_p = 1$ s, and $T_p = 0.25$ s, respectively. For broadband dynamical decoupling, five π pulses are inserted into each probe at random times such that the average π pulse frequency $f_\pi = 20$ Hz. For narrowband dynamical decoupling, the π pulse frequency is different for each probe and is selected from a uniform random distribution ranging from 2 Hz to 20 Hz. These are selected to optimize the sensitivity in both cases to oscillations between 1 and 10 Hz. For each measurement protocol, we simulate at least 100 measurements for dynamical decoupling algorithms and 1000 measurements for the differential spectroscopy case and fit to obtain the maximum amplitude of the theoretical dark matter line shape with 95% confidence.

Fractional frequency uncertainty plots are presented in Fig. 2. Differential spectroscopy rapidly loses sensitivity at frequencies above $f_{\mathrm{DM}} = 1/T_p$ due to more than one dark matter oscillation fitting into the probe time. Narrowband dynamical decoupling achieves sensitivity for higher dark matter masses. Broadband dynamical decoupling offers comparable sensitivity to NBDD with a lower probe time T_p which is uniform throughout the large range of masses unlike either DS or NBDD. Most importantly, we clearly demonstrate that BBDD reaches the 10^{-13} DM mass range without a significant loss of sensitivity, critical to a recent proposal to search for a DM halo bound to the Sun [10].

Figure 2 shows results for two different levels of laser frequency noise, and BBDD is shown to be less sensitive to laser frequency noise than NBDD. This is because in NBDD, each probe is sensitive to both signal and laser noise at only one frequency. Thus, the laser noise contribution to the measurement at each oscillation frequency is averaged over only a small fraction of the total probes of the measurement. In

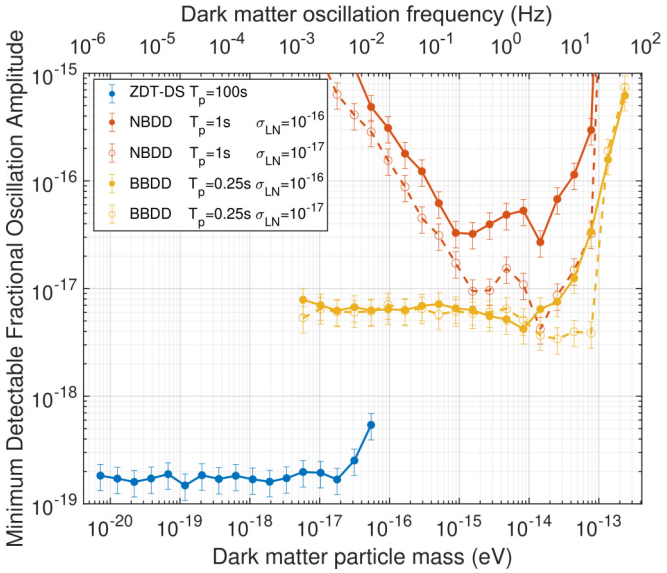

FIG. 2. Smallest detectable fractional frequency amplitude of oscillating clock frequencies due to dark matter for differential spectroscopy, narrowband dynamical decoupling, and broadband dynamical decoupling. The sensitivity of the dynamical decouping algorithms depends strongly on the laser frequency noise, which is set to different levels for the filled and open circles.

contrast, in BBDD each probe is sensitive to both signal and laser noise at all frequencies simultaneously. Quantitatively, in Eq. (12), the signal $\langle(\phi_S)^2\rangle^{1/2}$ is proportional to the number of probes in the measurement that are sensitive to any particular frequency, whereas with the noise $\langle(\phi_N)^2\rangle^{1/2}$ grows with a smaller power that depends on the spectrum of the laser noise. Hence, the signal-to-noise ratio is lower for BBDD than for NBDD because more probes are sensitive to noise at each frequency.

BBDD also relaxes the required fidelity of the π pulses. In our NBDD simulations, up to 19 π pulses are inserted into the Ramsey sequence. In our BBDD simulations, only five π pulses are inserted into the Ramsey sequence. In either case, the π pulse infidelity times the number of π pulses per probe must be much smaller than one. Trapped-ion optical qubits have achieved π pulses with an infidelity of 5×10^{-3} [35].

An exclusion plot for d_e presented in Fig. 3 shows an improvement in sensitivity by many orders of magnitude with nuclear clock experiments. For higher dark matter masses, only the proposed 1-km atom MAGIS interferometer [4] offers a sensitivity similar to that of a tabletop nuclear clock with dynamical decoupling.

IV. ELECTRON BRIDGE TWO-PHOTON SPECTROSCOPY

Isolated $^{229}\mathrm{Th}^{3+}$ions are expected to have a very long isomer half-life of 1740(50) s for a nucleus isolated in a vacuum [40]. The electronic and nuclear energy-level structure of $^{229}\mathrm{Th}^{3+}$is shown in Fig. 4. For spectroscopy sequence durations that approach the lifetime limit of the isomer state, a natural choice of the electronic state for nuclear spectroscopy is the $5F_{5/2}$ electronic ground state [16]. In this case, the nuclear transition is most naturally driven using a single 148-nm photon. Although significant progress has been made towards

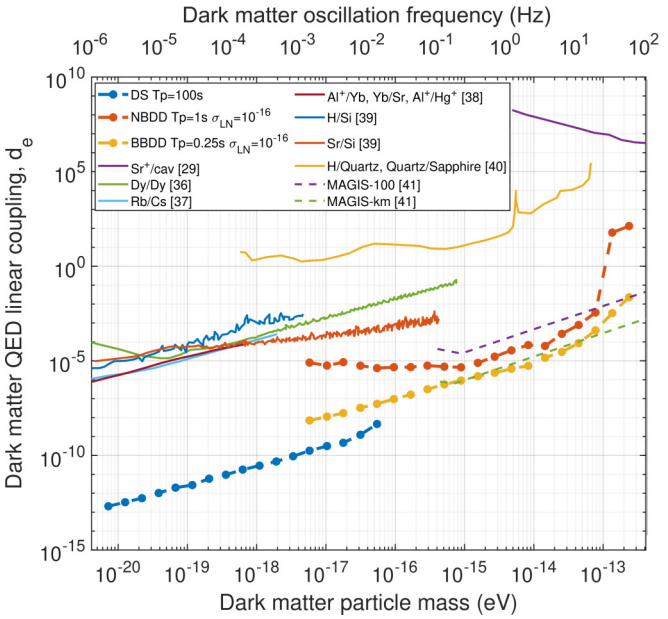

FIG. 3. Exclusion plot for the linear coupling constant of scalar dark matter to the QED electromagnetic field tensor. Coupling constants above the solid lines have already been ruled out by previous experiments [7,8,29,36–38]. Plotted circles show the simulated sensitivities of searches based on thorium nuclear clocks. The three quantum metrology algorithms considered here are shown. Other proposed experiments are shown as dashed lines [39]. More details of these lines can be found in Ref. [4].

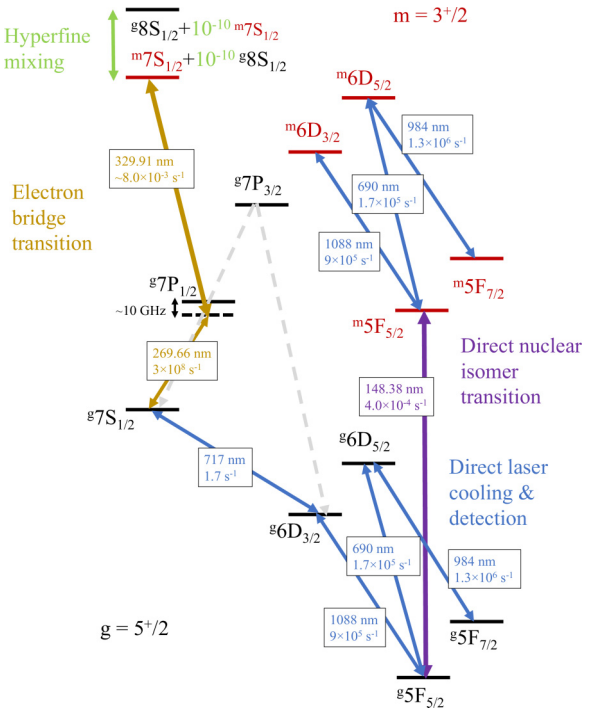

FIG. 4. Energy level diagram of $^{229}Th^{3+}$isomer showing two methods of driving the clock transition. Einstein A coefficients for the transitions are listed based on the values in Ref. [46]. The direct nuclear isomer transition wavelength and lifetime are from [19], while the wavelength of the $7P_{1/2}$-$7S_{1/2}$ transition is obtained from [45]. The electron bridge transition wavelength is calculated using these values.

constructing narrow linewidth lasers at this wavelength [41], these lasers are very challenging and have limited up-time.

An alternative method is two-photon electron-bridge spectroscopy [42,43]. Starting from the metastable $^g7S_{1/2}$ electronic excited state (where the g superscript indicates the nuclear ground state), a two-photon transition to the nuclear excited state $^m7S_{1/2}$ can be driven using $^g7P_{1/2}$ as an intermediate state. The second step of this transition is enhanced because $^m7S_{1/2}$ contains a small admixture of the $^g8S_{1/2}$ state with an estimated amplitude of $\sim 10^{-5}$ [43]. The electron-bridge technique shifts the required laser wavelength from the very challenging VUV near 148 nm up to less challenging UV wavelengths of 270 nm and 330 nm.

For precision nuclear spectroscopy using the electron-bridge technique, we propose detuning by ~10 GHz from the intermediate state and driving off-resonant two-photon transitions [44]. For sufficiently low Rabi frequencies, the $^g7P_{1/2}$ is not populated and the spectroscopic coherence time will be limited by the 0.6 s electronic decay lifetime of the $7S_{1/2}$ state [45]. This is sufficient for dynamical decoupling sequence durations up to a few hundred ms that are well suited for searches for dark matter oscillations in the 0.1 to 1 kHz frequency range. Table I compares various parameters in direct and electron bridge excitation methods.

V. DISCUSSION

Ultralight scalar dark matter is highly theoretically motivated and there has been an increased interest in searches for such dark matter candidates. Thorium-based nuclear clock experiments will offer better sensitivity to ultralight scalar dark matter than any other existing or proposed experiment by many orders of magnitude for a large range of dark matter masses. Although differential spectroscopy offers an excellent scheme for such experiments for a lower dark matter mass range, for $f > 1/T_p$ sensitivity is greatly reduced owing to many dark matter oscillations being packed within the probe time of the experiment. Dynamical decoupling sequences offer a solution and offer increased sensitivity for higher dark matter masses within the ultralight dark matter mass range, matched only by the proposed MAGIS-km experiment. Broadband dynamical decoupling, in particular, offers all these advantages, with sensitivity not being dependent on the probe time, so lower probe times can be used when

TABLE I. Comparison of direct and electron bridge excitation methods.

	Direct	Electron bridge	
Laser wavelength (nm)	148	270	330
Laser power (W)	10^{-6}	10^{-8}	1
$1/e^2$ beam radius (μm)	10	30	3
Detuning (GHz)		10	
Min. π pulse duration (ms)	40	4	
Coherence time (s)	10^3	0.6	
Spont. emis. prob. per pulse		0.02	

employing this scheme. We developed detailed simulations of clock experiments searching for ultralight scalar dark matter via α variations, which include dark matter decoherence, laser noise, and quantum projection noise. Using these simulations, we demonstrate that broadband dynamical decoupling exhibits reduced sensitivity to laser noise. Consequently, over a broad range of masses, it provides comparable sensitivity to ultralight scalar dark matter, regardless of whether the laser noise level is at 10^{-16} or 10^{-17}.

Our simulations show the superiority of the differential spectroscopy approach when searching for lower-frequency signals. However, we are interested in how to search for higher frequencies, where dynamical decoupling is better suited. Figure 2 shows that the performance of BBDD is better than that of NBDD, for the parameters that we chose to search for a signal of an unknown frequency. Once the frequency of the signal, in this case ultralight scalar dark matter, is known, NBDD would be better suited with a narrower frequency range and we expect better performance than given here.

The broadband dynamical decoupling algorithm proposed here is a general technique that can be used to search for frequency or phase oscillations of atomic transition frequencies or qubit transition frequencies in other platforms, for example, due to decoherence or new physics, where the oscillation frequency is unknown. One important difference from previous work is that all of the pulses are analyzed coherently. BBDD could, for instance, be used in laser frequency noise measurements similar to the work of Bishof *et al.* [47]. The frequency stability of lasers is typically characterized by measuring the beat note of the laser under test with a more stable reference laser. However, for state-of-the-art clock lasers a more stable reference laser is often unavailable. In this case, the frequency stability of the clock laser can be characterized using the atoms of an optical clock as the more stable reference, and the broadband dynamical decoupling algorithm provides a technique for performing laser frequency noise characterization at noise frequencies higher than is possible with conventional Ramsey spectroscopy.

ACKNOWLEDGMENTS

The authors thank J. Valencia and D. A. Hite for critical reading of the manuscript. This work was supported by the Army Research Office (Grant No. W911NF-20-1-0135), the National Institute of Standards and Technology, the National Science Foundation Q-SEnSE Quantum Leap Challenge Institute (Grant No. OMA-2016244), the Office of Naval Research (Grant No. N00014-20-1-2513), the NSF award 2326810 and the European Research Council (ERC) under the European Union's Horizon 2020 research and innovation program (Grant No. 856415). This research was supported in part through the use of University of Delaware HPC Caviness and DARWIN computing systems: DARWIN is a resource for computational and data-intensive research at the University of Delaware and in the Delaware region [48].

APPENDIX A: DARK MATTER DECOHERENCE

We treat the dark matter field as stochastic, rather than deterministic, based on the approach of Ref. [49]. This approach accounts for dark matter decoherence and hence is more appropriate than a deterministic model for higher frequency dark matter, which corresponds to smaller coherence times. For stochastic fields, the power spectral density is not merely a delta function at the Compton frequency, but is distributed around it. It is proportional to the lineshape

$$F(\omega) = (2\pi)^{-1/2}\tau_c\eta^{-1}e^{-\eta^2}e^{-(\omega-2\pi f_{\rm DM})\tau_c} \times \sinh\{\eta\sqrt{(}\eta^2 + 2[\omega - 2\pi f_{\rm DM})\tau_c]\}. \quad \text{(A1)}$$

Here η is the ratio of galactic velocity and $v_{\rm vir}$ which is the virial velocity of the dark matter halo, which is taken to be 1, while $\tau_c \sim \lambda_{\rm DM}/v_{\rm vir} = h/(m_\phi v_{\rm vir}^2) = c^2/(f_{\rm DM}v_{\rm vir}^2) = 10^6/f_{\rm DM}$ is the coherence time, and $\lambda_{\rm DM}$ and $f_{\rm DM}$ are the dark matter Compton wavelength and frequency, respectively. The analysis frequency f is taken to correspond to all $\omega = 2\pi f$ for which $F(\omega)$ is nonzero.

The power spectral density of the dark matter field can be obtained using the line profile according to

$$\langle|\tilde{\phi}_p|^2\rangle = \frac{\pi N_f}{dt}\phi_0^2 F(\omega_p). \quad \text{(A2)}$$

Here N_f is the number of points taken in frequency space to have 1000 points on the dark matter line and $dt = 0.1/f_{\rm DM}$ is the sampling interval chosen to be appropriately small.

Random coefficients in the frequency domain are obtained by randomly generating normally distributed complex numbers $\frac{\tilde{\phi}_p}{\phi_0} = \sqrt{\frac{1}{2}\frac{\langle|\tilde{\phi}_p|^2\rangle}{(\phi_0)^2}}e^{2\pi ij}$, where j is a uniformly distributed random number between 0 and 1. Finally, the amplitude $v_{S,j}$ and phase θ_j of the oscillating signal in the time domain are obtained by $\frac{\phi_j}{\phi_0} = \frac{2}{N_f}\sum_p \frac{\tilde{\phi}_p}{\phi_0}e^{i(\omega_p-\omega_{\rm DM})t}$, resulting in

$$\phi_{S,j} = \int_{t_j-T_p/2}^{t_j+T_p/2} 2\pi g(t) v_{S,j}\cos(2\pi f t + \theta_j)dt. \quad \text{(A3)}$$

APPENDIX B: DARK MATTER LINESHAPE

The expected lineshape of the dark matter signal is obtained by convolving Eq. (A1) with the absolute value of the sinc function

$$F_c = 4\pi\int F(f-f')\,\text{abs}\{\text{sinc}[(f'-f-f_{\rm DM})\,T_m]\}\,df'. \quad \text{(B1)}$$

Here, f' is the independent variable for integration and taken to be a large number of values ranging from $-1000/T_m$ to $1000/T_m$ for numerical evaluation of the integral. We take the number of values to be $N_i = 10^5$ if the integration time T_m is greater than the decoherence time τ_c, otherwise $N_i = 10^6$.

If the interrogation time is significantly lower than the coherence time, $T_m < 0.1\tau_c$, we do not use the lineshape (A1) and instead just use the sinc function

$$F_c = \text{abs}\{\text{sinc}[(f - f_{\rm DM})\,T_m]\}, \quad \text{(B2)}$$

where $\omega_{\rm DM}$ is the dark matter angular frequency.

The lineshape from the simulation ϕ_S comes from Eq. (11) where the contribution due to dark matter in the jth probe $\phi_{S,j}$ is given by Eq. (10). The simulated signal is fitted onto the expected line shape using the fmincon function in MATLAB,

where the function minimized is the mean square error

$$\mathrm{MSE}(p_1, p_2) = \mathrm{mean}\Big(\Big(\sqrt{p_1^2\, F_c^2 + p_2^2} - \phi_M\Big)^2\Big). \tag{B3}$$

The initial guesses for inputs p_1 and p_2 are taken to be $\max(F_c)\max(\phi_S)$ and $\sqrt{T_m/T_p}/4$, respectively. The fmincon function finds the values p_1 and p_2 which minimize the mean square error.

APPENDIX C: LASER NOISE

We introduce a method for numerical generation of time-series random numbers with a power-law spectrum $S = S_0 f^{\lambda}$, which is used to generate pink laser frequency noise for simulating dynamical decoupling sequences in this work ($\lambda = -1$). The scale $S_0 = 1/\sqrt{2\log 2}$ is chosen so that pink noise is produced with an Allan deviation of 1 at an averaging time of 1 s. A Mandelbrot state-space noise model is used. We generate a model of size $m = 10$ to approximate the desired spectrum from a minimum frequency $f_{\mathrm{Min}} = 10^{-6}$ Hz to a maximum frequency $f_{\mathrm{Max}} = 10^{3}$ Hz. The elements of the transition matrix A, the input vector B, and the output vector C are given by

$$A(i,i) = \exp\left(-\beta^{i-1}\frac{dt}{\alpha\tau}\right), \tag{C1}$$

$$B(i,1) = \frac{1-\exp\left(-\beta^{i-1}\frac{dt}{\alpha\tau}\right)}{\beta^{i-1}}, \quad \text{and} \tag{C2}$$

$$C(1,i) = S_0\frac{1}{\sqrt{2}}\alpha^{\frac{6-\lambda}{8}}(f_{\mathrm{Min}}dt)^{\lambda/2} \times \prod_{j=1,j\neq i}^{m}(\alpha-1)\frac{\beta^{i-1}}{\alpha^m}\frac{\alpha\beta^{j-1}-\beta^{i-1}}{\beta^{j-1}-\beta^{i-1}}. \tag{C3}$$

Here, index i goes from 1 to m, dt is the time step chosen to be an appropriately small fraction of the probe time, $\tau = 1/(2\pi f_{\mathrm{Min}})$, $\beta = (10 f_{\mathrm{Max}}/f_{\mathrm{Min}})^{1/m}$, and $\alpha = \beta^{-\lambda/2}$. The state vector z for timestep j is obtained from the one for timestep $j-1$ according to the update equation

$$z_j = A\, z_{j-1} + B\, r, \tag{C4}$$

where r is an m element vector of normally distributed random numbers, which are regenerated for each j. The state vector is used to generate the time series of random numbers according to

$$y_j = C\, z_j. \tag{C5}$$

This method requires less memory than other techniques based on Fourier transforming white noise.

The laser noise frequencies are computed as $\nu_{LN} = \nu_0 \times \sigma_{LN} \times y_j$, where $\nu_0 = c/\lambda_0$ is the laser frequency, with $\lambda_0 = 148.3821(5)$ nm, and $\sigma_{LN} = 10^{-16}$ or $\sigma_{LN} = 10^{-17}$ is the Allan deviation of the pink laser noise.

[1] A. D. Ludlow, M. M. Boyd, J. Ye, E. Peik, and P. O. Schmidt, Rev. Mod. Phys. **87**, 637 (2015).
[2] S. M. Brewer, J.-S. Chen, A. M. Hankin, E. R. Clements, C. W. Chou, D. J. Wineland, D. B. Hume, and D. R. Leibrandt, Phys. Rev. Lett. **123**, 033201 (2019).
[3] A. Banerjee, G. Perez, M. Safronova, I. Savoray, and A. Shalit, J. High Energy Phys. 10 (2023) 042.
[4] D. Antypas, A. Banerjee, C. Bartram, M. Baryakhtar, J. Betz, J. Bollinger, C. Boutan, D. Bowring, D. Budker, D. Carney *et al.*, arXiv:2203.14915.
[5] A. Derevianko and M. Pospelov, Nat. Phys. **10**, 933 (2014).
[6] A. Arvanitaki, J. Huang, and K. Van Tilburg, Phys. Rev. D **91**, 015015 (2015).
[7] K. Van Tilburg, N. Leefer, L. Bougas, and D. Budker, Phys. Rev. Lett. **115**, 011802 (2015).
[8] A. Hees, J. Guéna, M. Abgrall, S. Bize, and P. Wolf, Phys. Rev. Lett. **117**, 061301 (2016).
[9] A. Banerjee, D. Budker, J. Eby, H. Kim, and G. Perez, Commun. Phys. **3**, 1 (2020).
[10] Y.-D. Tsai, J. Eby, and M. S. Safronova, Nat. Astron. **7**, 113 (2023).
[11] T. Damour and J. F. Donoghue, Phys. Rev. D **82**, 084033 (2010).
[12] V. A. Dzuba and V. V. Flambaum, Can. J. Phys. **87**, 15 (2009).
[13] V. V. Flambaum, Phys. Rev. Lett. **97**, 092502 (2006).
[14] K. Beeks, G. Kazakov, F. Schaden, I. Morawetz, L. de Col, T. Riebner, M. Bartokos, T. Sikorsky, T. Schumm, C. Zhang, T. Ooi, J. Higgins, J. Doyle, J. Ye, and M. Safronova, arXiv:2407.17300.
[15] E. Peik and C. Tamm, Europhys. Lett. **61**, 181 (2003).
[16] C. J. Campbell, A. G. Radnaev, A. Kuzmich, V. A. Dzuba, V. V. Flambaum, and A. Derevianko, Phys. Rev. Lett. **108**, 120802 (2012).
[17] J. Berengut and V. Flambaum, in *Journal of Physics: Conference Series*, (IOP, New York, 2011), Vol. 264, p. 012010.
[18] E. Peik, T. Schumm, M. Safronova, A. Palffy, J. Weitenberg, and P. G. Thirolf, Quantum Sci. Technol. **6**, 034002 (2021).
[19] J. Tiedau, M. V. Okhapkin, K. Zhang, J. Thielking, G. Zitzer, E. Peik, F. Schaden, T. Pronebner, I. Morawetz, L. T. De Col, F. Schneider, A. Leitner, M. Pressler, G. A. Kazakov, K. Beeks, T. Sikorsky, and T. Schumm, Phys. Rev. Lett. **132**, 182501 (2024).
[20] R. Elwell, C. Schneider, J. Jeet, J. E. S. Terhune, H. W. T. Morgan, A. N. Alexandrova, H. B. Tran Tan, A. Derevianko, and E. R. Hudson, Phys. Rev. Lett. **133**, 013201 (2024).
[21] C. Zhang, T. Ooi, J. S. Higgins, J. F. Doyle, L. von der Wense, K. Beeks, A. Leitner, G. A. Kazakov, P. Li, P. G. Thirolf, T. Schumm, and J. Ye, Nature (London) **633**, 63 (2024).
[22] D. B. Hume and D. R. Leibrandt, Phys. Rev. A **93**, 032138 (2016).
[23] M. E. Kim, W. F. McGrew, N. V. Nardelli, E. R. Clements, Y. S. Hassan, X. Zhang, J. L. Valencia, H. Leopardi, D. B. Hume, T. M. Fortier, A. D. Ludlow, and D. R. Leibrandt, Nat. Phys. **19**, 25 (2023).
[24] E. L. Hahn, Phys. Rev. **80**, 580 (1950).
[25] L. Viola and S. Lloyd, Phys. Rev. A **58**, 2733 (1998).
[26] H. Y. Carr and E. M. Purcell, Phys. Rev. **94**, 630 (1954).
[27] S. Meiboom and D. Gill, Rev. Sci. Instrum. **29**, 688 (1958).

[28] S. Kotler, N. Akerman, Y. Glickman, A. Keselman, and R. Ozeri, Nature (London) **473**, 61 (2011).
[29] S. Aharony, N. Akerman, R. Ozeri, G. Perez, I. Savoray, and R. Shaniv, Phys. Rev. D **103**, 075017 (2021).
[30] A. Quessada, R. P. Kovacich, I. Courtillot, A. Clairon, G. Santarelli, and P. Lemonde, J. Opt. B: Quantum Semiclass. Opt. **5**, S150 (2003).
[31] G. P. Centers, J. W. Blanchard, J. Conrad, N. L. Figueroa, A. Garcon, A. V. Gramolin, D. F. J. Kimball, M. Lawson, B. Pelssers, J. A. Smiga *et al.*, Nat. Commun. **12**, 7321 (2021).
[32] R. Shaniv and R. Ozeri, Nat. Commun. **8**, 14157 (2017).
[33] E. B. Wilson, J. Am. Stat. Assoc. **22**, 209 (1927).
[34] O. McGrath and K. Burke, Am. Stat. **78**, 437 (2024).
[35] L. Postler, S. Heußen, I. Pogorelov *et al.*, Nature (London) **605**, 675 (2022).
[36] K. Beloy *et al.*, Nature (London) **591**, 564 (2021).
[37] C. J. Kennedy, E. Oelker, J. M. Robinson, T. Bothwell, D. Kedar, W. R. Milner, G. E. Marti, A. Derevianko, and J. Ye, Phys. Rev. Lett. **125**, 201302 (2020).
[38] W. M. Campbell, B. T. McAllister, M. Goryachev, E. N. Ivanov, and M. E. Tobar, Phys. Rev. Lett. **126**, 071301 (2021).
[39] M. Abe, P. Adamson, M. Borcean, D. Bortoletto, K. Bridges, S. P. Carman, S. Chattopadhyay, J. Coleman, N. M. Curfman, K. DeRose *et al.*, Quantum Sci. Technol. **6**, 044003 (2021).
[40] S. Kraemer *et al.*, Nature (London) **617**, 706 (2023).
[41] C. Benko, T. K. Allison, A. Cingöz, L. Hua, F. Labaye, D. C. Yost, and J. Ye, Nat. Photonics **8**, 530 (2014).
[42] S. G. Porsev, V. V. Flambaum, E. Peik, and C. Tamm, Phys. Rev. Lett. **105**, 182501 (2010).
[43] S. G. Porsev and V. V. Flambaum, Phys. Rev. A **81**, 032504 (2010).
[44] D. J. Wineland, C. Monroe, W. M. Itano, D. Leibfried, B. E. King, and D. M. Meekhof, J. Res. Natl. Inst. Stand. Technol. **103**, 259 (1998).
[45] A. G. Radnaev, C. J. Campbell, and A. Kuzmich, Phys. Rev. A **86**, 060501 (2012).
[46] M. S. Safronova and U. I. Safronova, Phys. Rev. A **87**, 062509 (2013).
[47] M. Bishof, X. Zhang, M. J. Martin, and J. Ye, Phys. Rev. Lett. **111**, 093604 (2013).
[48] R. Eigenmann, B. E. Bagozzi, A. Jayaraman, W. Totten, and C. H. Wu, *DARWIN-A Resource for Computational and Data-intensive Research at the University of Delaware and in the Delaware Region* (Data Science Institute, University of Delaware, Newark, DE, 2021), https://udspace.udel.edu/handle/19716/29071.
[49] A. Derevianko, Phys. Rev. A **97**, 042506 (2018).